Department of Mathematics and Systems Analysis

Computational approaches in electrical impedance tomography with applications to head imaging

Valentina Candiani

Aalto University

DOCTORAL DISSERTATIONS

Aalto University publication series
DOCTORAL DISSERTATIONS 139/2021

Computational approaches in electrical impedance tomography with applications to head imaging

Valentina Candiani

A doctoral dissertation completed for the degree of Doctor of Science (Technology) to be defended, with the permission of the Aalto University School of Science, at a public examination held at the lecture hall M1 of the school on 12 November 2021 at 13.

Aalto University
School of Science
Department of Mathematics and Systems Analysis

Supervising professor
Prof. Nuutti Hyvönen

Thesis advisor
Prof. Nuutti Hyvönen

Preliminary examiners
Prof. Lucas Chesnel, École Polytechnique, France
Prof. Sarah J. Hamilton, Marquette University, USA

Opponent
Prof. Erkki Somersalo, Case Western Reserve University, USA

Aalto University publication series
DOCTORAL DISSERTATIONS 139/2021

© 2021 Valentina Candiani

ISBN 978-952-64-0544-5 (printed)
ISBN 978-952-64-0545-2 (pdf)
ISSN 1799-4934 (printed)
ISSN 1799-4942 (pdf)
http://urn.fi/URN:ISBN:978-952-64-0545-2

Unigrafia Oy
Helsinki 2021

Finland

Printed matter
4041-0619

Aalto University

Abstract

Aalto University, P.O. Box 11000, FI-00076 Aalto www.aalto.fi

Author
Valentina Candiani

Name of the doctoral dissertation
Computational approaches in electrical impedance tomography with applications to head imaging

Publisher School of Science

Unit Department of Mathematics and Systems Analysis

Series Aalto University publication series DOCTORAL DISSERTATIONS 139/2021

Field of research Mathematics

Manuscript submitted 15 June 2021 **Date of the defence** 12 November 2021

Permission for public defence granted (date) 13 September 2021 **Language** English

☐ **Monograph** ☒ **Article dissertation** ☐ **Essay dissertation**

Abstract

This thesis considers computational approaches to address the inverse problem arising from electrical impedance tomography (EIT), where the aim is to reconstruct (useful information about) the conductivity distribution inside a physical body from boundary measurements of current and voltages. The problem is nonlinear and highly ill-posed, and it generally presents several theoretical and numerical challenges. In fact, the search for a solution usually requires either carefully selected regularization techniques or simplifying assumptions on the measurement setting.

A particular focus is on applying EIT to stroke detection in medical imaging, where measurement and modelling errors considerably deteriorate the available boundary data. To model these uncertainties, a novel computational three-dimensional head model is introduced and utilized to simulate realistic synthetic electrode measurements. According to the studied application, different models for the forward problem are considered, such as the *continuum model*, the *complete electrode model* and its smoothened version. The examined solution strategies correspond to different methodologies, ranging from regularized iterative reconstruction algorithms to machine learning techniques. The performance of these methods is assessed via three-dimensional simulated experiments performed in different settings.

Keywords Inverse problems, electrical impedance tomography, complete electrode model, computational head model, stroke detection, Bayesian inversion, modeling errors, inclusion detection, neural networks

ISBN (printed) 978-952-64-0544-5 **ISBN (pdf)** 978-952-64-0545-2

ISSN (printed) 1799-4934 **ISSN (pdf)** 1799-4942

Location of publisher Helsinki **Location of printing** Helsinki **Year** 2021

Pages 162 **urn** http://urn.fi/URN:ISBN:978-952-64-0545-2

Preface

This work has been carried out during the years 2017–2021 at the Department of Mathematics and Systems Analysis of Aalto University. I acknowledge the Academy of Finland and the Finnish Cultural Foundation for funding my research during these years.

I want to express my deepest gratitude to Nuutti Hyvönen for his patient guidance and help during my doctoral studies. He has been an excellent supervisor, not only for his mathematical expertise but also for supporting me even in the difficult and unprecedented pandemic times.

I am grateful to Jari Kaipio for giving me the opportunity to work with him at University of Auckland, for being an incredible host and for driving me around through breathtaking sites in New Zealand. I owe special thanks to my collaborators Jérémi Dardé, Henrik Garde, Antti Hannukainen, Ville Kolehmainen and Matteo Santacesaria for always thought-provoking discussions and for their significant contributions to the articles that constitute this thesis. I am thankful to my preliminary examiners Sarah Jane Hamilton and Lucas Chesnel for taking the time to carefully review the manuscript, and to Erkki Somersalo for agreeing to act as my opponent in the public examination.

I would like to thank my colleagues at the department, the applied math group and in particular the “coffee gang” for many entertaining conversations and for making my stay at Aalto an amazing journey. I am grateful to all the friends I have met in Finland, with whom I have had the pleasure of sharing wonderful experiences, even through the dark Finnish winters. I thank my friends of a lifetime in Italy, my sister Silvia and my parents Carlo and Paola for their endless support, even from far away. Finally, a special thanks to Marco for always being there for me.

Helsinki, October 1, 2021,

Valentina Candiani

Contents

List of Publications

This thesis consists of an overview and of the following publications which are referred to in the text by their Roman numerals.

I V. Candiani, A. Hannukainen and N. Hyvönen. Computational framework for applying electrical impedance tomography to head imaging. *SIAM Journal on Scientific Computing*, 41(5), B1034–B1060, October 2019.

II V. Candiani, J. Dardé, H. Garde and N. Hyvönen. Monotonicity-based reconstruction of extreme inclusions in electrical impedance tomography. *SIAM Journal on Mathematical Analysis*, 52(6), 6234–6259, December 2020.

III V. Candiani and M. Santacesaria. Neural networks for classification of strokes in electrical impedance tomography on a 3D head model. *Mathematics in Engineering*, 4(4), 1–22, August 2021.

IV V. Candiani, N. Hyvönen, J. P. Kaipio and V. Kolehmainen. Approximation error method for imaging the human head by electrical impedance tomography. *arXiv:2106.06238*, 24 pages, June 2021.

Author's contributions

Publication I: "Computational framework for applying electrical impedance tomography to head imaging"

The adaptation of the computational head model and the FEM solver (provided by Hannukainen) for the smoothened complete electrode model and the numerical approximation of the Fréchet derivatives are mainly due to the author. She also implemented the reconstruction algorithm and shared the main responsibility for the writing process with Hyvönen.

Publication II: "Monotonicity-based reconstruction of extreme inclusions in electrical impedance tomography"

The author contributed to proving the main theoretical results as an equal member of the research team. She also participated in the writing process.

Publication III: "Neural networks for classification of strokes in electrical impedance tomography on a 3D head model"

The implementation of the three-layer computational head model, the generation of the datasets, and the training and testing of the considered networks are due to the author. She also substantially contributed to the writing process, designing the experiments and reporting their results.

Publication IV: "Approximation error method for imaging the human head by electrical impedance tomography"

The implementation of the three-layer computational head model and the

generation of the approximation error statistics are mainly due to the author. She also significantly contributed to the implementation of the reconstruction algorithm and to the writing process. In particular, she designed and reported the numerical experiments.

Abbreviations

2D Two-Dimensional

3D Three-Dimensional

AutoML Automatic Machine Learning

BCE Binary Cross Entropy

CEM Complete Electrode Model

CM Continuum Model

CNN Convolutional Neural Network

CT Computed Tomography

DN Dirichlet-to-Neumann

EIT Electrical Impedance Tomography

FCNN Fully Connected Neural Network

FE Finite Element

FEM Finite Element Method

MAP Maximum A Posteriori

MRI Magnetic Resonance Imaging

ND Neumann-to-Dirichlet

NN Neural Network

ReLU Rectified Linear Unit

TV Total Variation

1. Introduction

Electrical impedance tomography (EIT) is a noninvasive imaging method that is based on current and voltage measurements on the boundary of an examined physical body. Typically, conducting surface electrodes drive low-frequency currents into the object under examination, the corresponding voltages are recorded and the measurement is repeated for a specified set of current patterns. Such boundary measurements depend on the interior conductivity of the object, and the aim of any algorithm designed for EIT is to reconstruct useful information about its distribution by (partially) inverting this dependence.

Applications of EIT arise from the fact that the values of the internal electrical conductivity vary considerably depending on the different materials or the anatomical tissues of the body under investigation, and reconstructing this spatial distribution allows one to detect changes and possible abnormalities. For instance, the conductivity of air, blood, bone, cancer and healthy tissues can differ significantly, enabling EIT to be well-suited for various medical applications, among which are pulmonary imaging, breast cancer detection and brain imaging [17]. In addition to diagnostics, EIT has several other applications, for example in nondestructive testing of materials in industrial environments and imaging of geologic structures. For further information about the potential uses of EIT, we refer to the review articles [13, 23, 95] and the references therein.

The introduction of EIT as a medical imaging technique dates back to 1978 and it is documented in a publication by Henderson and Webster [49]. However, the first practical realization of a clinical impedance tomography system was developed only in 1984 by David C. Barber and Brian H. Brown [10]. EIT provides several potential advantages over other imaging methods. It is a relatively inexpensive, noninvasive and fast technique, and there are no established dangers connected to its use. The major drawback that characterizes this method is, however, its low spatial resolution. Previous and more conventional imaging modalities, such as X-ray computed tomography (CT) and magnetic resonance imaging (MRI), are capable of imaging anatomical structures with an extremely

high accuracy, an advantage that in many diagnostic cases outweighs the expense and the inflexibility of these methods. Unlike X-rays traveling linearly through an object, the electric currents used in EIT propagate throughout the whole (three-dimensional) subject, a characteristic that makes the inverse problem related to EIT less well defined than those of CT or MRI, hence resulting in a relatively poor spatial resolution. Nonetheless, its advantages enable EIT to be of potential importance for bedside monitoring, alongside other imaging modalities, for emergency use, or in locations where large scanners are too expensive or impractical.

The lack of spatial resolution is explained by the ill-posedness of the inverse problem of EIT, i.e. the so-called inverse conductivity problem. According to the definition given by Jacques Hadamard in 1923 [40], a mathematical model of a physical problem is well posed if it has a unique solution that depends continuously on the data. Conversely, in an ill-posed problem the solution may not exist or there could be several (possibly infinitely many) of them. Moreover, even if a solution exists, it may not depend continuously on the data in any reasonable metric. In the setting of EIT, the last condition means that there are arbitrarily many conductivity distributions that can produce (almost) equivalent electrode voltages. Therefore, a complete knowledge of electrode measurement data does not necessarily yield enough information on the underlying conductivity distribution, causing EIT to be extremely sensitive to measurement noise and modeling errors, which are unavoidable in practical applications.

For these reasons, one research direction in this field is developing inversion algorithms capable of handling mismodeling of the domain, geometric inaccuracies and errors in the measurement setup. To deal with the inherent ill-posedness of the problem, one can introduce (ad-hoc) prior information in order to constrain the solution so that the uncontrolled variations causing the instability are ruled out. To be more precise, the numerical challenges are usually managed by resorting to regularization techniques designed for inverse problems or Bayesian methods applied to a statistical formulation of the considered problem.

On the other hand, one can address the inverse conductivity problem of EIT from some different perspectives, depending on the application at hand. In some cases, simplifying the assumptions and thus reducing the complexity of the problem may well be a way to circumvent some of the aforementioned issues. One possible strategy is to resort to the easier problem of *inclusion detection*, with the goal of retrieving information on (the location of) an unknown conductivity perturbation in a known background. Another feasible research direction is the exploration of machine learning techniques to either speed up the reconstruction process or to provide a simple tool for determining if the examined body presents an anomaly.

Outline of the dissertation

In this work we focus specifically on applying EIT as a brain imaging modality aimed at stroke detection. Stroke, a serious and acute cerebrovascular disease, can be of two types: *hemorrhagic*, when caused by a blood vessel rupture and the consequent accumulation of blood in the tissue around it, or *ischemic*, if provoked by lack of blood flow to the brain tissue caused by a blood clot [30, 83, 100]. Due to the difference in blood concentration in the tissues affected by a stroke, mapping the conductivity distribution of the brain represents a potential tool to quickly detect, localize and classify the ongoing seizure.

To this end, the main research topics of this dissertation are: (i) to implement a 3D head model acting as the studied domain for stroke detection and allowing variations in head shapes and sizes, (ii) to develop absolute EIT reconstruction algorithms able to tolerate uncertainty in the measurement geometry, and (iii) to investigate, under simplifying assumptions, other computational approaches aimed at stroke classification. While introducing a model for the forward problem is by no means a trivial task, it falls outside the scope of this thesis, and we will therefore consider some well-established forward models.

In order to simulate electrode measurements and numerically solve the associated inverse problem, we introduce in Publication I a novel computational head model, where we utilize a library of fifty human heads from [71] and form a *principal component* model for the associated geometric variations. The model is successively refined in Publication III and IV to consider a more sophisticated head anatomy, where scalp and skull layers are also included.

Full reconstruction of the conductivity distribution for stroke detection is investigated in Publications I and IV, where the aim is to exploit EIT without accurate information on the electrode positions or the geometry of the examined patient's head. The functionality of some Newton-type reconstruction algorithms is investigated, together with two alternative methods designed to deal with geometric mismodeling. In Publication I, we employ the derivatives of the electrode potentials with respect to the exterior boundary shape and the electrode locations in a regularized Newton-type output least squares algorithm that simultaneously reconstructs all relevant unknowns in the measurement setup. In Publication IV, we include the error caused by the mismodeling as an extra additive noise process in the measurement model, which is then taken into account within the Bayesian inversion paradigm.

The monotonicity method for inclusion detection is studied in Publication II, under the (unrealistic) assumption of infinite-dimensional boundary data. This study is more theoretically oriented, as we prove how to extend the method to detect *extreme* inclusions, that is, parts of the studied domain

that are either perfectly conducting or perfectly insulating. However, due to its simplicity, the method also adapts in a natural way to more realistic electrode models, allowing for a straightforward numerical implementation [32, 33, 34, 47] applicable in principle to the aforementioned computational head model. Inclusion detection comprises a potential paradigm for applications that consider locating inhomogeneities inside objects with known background conductivities, for instance when considering bedside monitoring in the presence of previously acquired complete reconstructions.

Finally, in Publication III we explore a pure application-oriented scenario, with the study of some specifically designed neural networks trained to perform a binary stroke classification (hemorrhage and no hemorrhage). Utilizing these methods clearly limits the application of EIT to just stroke detection, without providing any information on its location. Nonetheless, the application of such techniques can considerably expedite the detection process and could be valuable in emergency use, if the reported symptoms clearly indicate the onset of a stroke and immediate treatment is needed, but the type of the stroke remains unknown.

2. Electrical impedance tomography

This section is devoted to presenting an overview of the mathematical fundamentals of EIT, with a particular focus on the application to head imaging; for more details about the existing theory and mathematical models, we refer to [13, 23, 95] and the references therein.

The mathematical description of the measurement setting is as follows. Let $\Omega \subset \mathbb{R}^d$, $d = 2, 3$, be a bounded domain representing the body under examination. We assume that Ω has a connected complement and a Lipschitz boundary $\partial\Omega$.

Our mathematical model for the propagation of currents in the body can be derived from Maxwell's equations for time-harmonic electromagnetic fields, under the assumption that the electric response of the body is linear and isotropic. Because in EIT applications the employed frequencies are relatively low, the quasi-static approximation of Maxwell's equations can be used to model the physical effects. It is also assumed that no internal current sources are present.

Under these assumptions, Ohm's law can be exploited to express the absence of current sources in an isotropic conductive medium, resulting in the conductivity equation

$$\nabla \cdot [\sigma(x)\nabla u(x)] = 0, \qquad x \in \Omega, \tag{2.1}$$

where $\sigma(x) > 0$ models the spatial conductivity distribution and $u(x)$ the interior electric potential. In the following, it is assumed that σ is a real-valued function, although most of the presented theory naturally extends to a complex-valued *admittivity* as well.

2.1 Continuum model

Several mathematical models have been developed to describe the EIT forward problem and to incorporate appropriate boundary conditions, including those introduced in [25, 89]. The simplest one is the *continuum model* (CM), which assumes infinite-dimensional boundary data. This

model formulation is useful for theoretical considerations, as in Publication II, but it does not typically result in accurate reconstructions as such because practical EIT measurement devices employ only a finite number of electrodes (with finite precision).

The idea behind the continuum model is that the application of a current density f on the boundary $\partial\Omega$ of the domain leads to the elliptic Neumann boundary value problem

$$\nabla \cdot (\sigma \nabla u) = 0 \quad \text{in} \quad \Omega, \qquad \sigma \frac{\partial u}{\partial \nu} = f \quad \text{on} \quad \partial\Omega, \tag{2.2}$$

where $\nu \in L^\infty(\partial\Omega, \mathbb{R}^d)$ is the outward unit normal of $\partial\Omega$ and the essential infimum of the conductivity inside the domain is assumed to be larger than zero, meaning that current can flow anywhere within Ω, i.e.

$$\sigma \in L^\infty_+(\Omega) = \Big\{ \sigma \in L^\infty(\Omega) : \operatorname*{ess\,inf}_{x\in\Omega} \sigma(x) > 0 \Big\}. \tag{2.3}$$

By applying standard theory of elliptic partial differential equations [38], it can be shown that for any given current density f in

$$H^{-1/2}_\diamond(\partial\Omega) = \Big\{ g \in H^{-1/2}(\partial\Omega) : \langle g, 1 \rangle_{\partial\Omega} = 0 \Big\},$$

the problem (2.2) has a solution $u \in H^1(\Omega)$ that is unique up to an additive constant, which is equivalent to choosing an earth point. The conservation of electrical charge, which states that the current density is conserved over the boundary, is accounted for in the "zero-mean" condition on f.

The ideal complete data for the EIT reconstruction problem corresponds to the knowledge of the full set of Cauchy data (pairs of current densities and voltages),

$$\Big\{ (f, u|_{\partial\Omega}) : u \text{ solves (2.2) for } f \in H^{-1/2}_\diamond(\partial\Omega) \Big\},$$

which can be characterized by the *Neumann-to-Dirichlet* (ND) map

$$\Lambda(\sigma) : H^{-1/2}_\diamond(\partial\Omega) \to H^{1/2}_\diamond(\partial\Omega)/\mathbb{R}, \qquad \Lambda(\sigma) : f \mapsto u^\sigma_f|_{\partial\Omega},$$

where $u^\sigma_f|_{\partial\Omega}$ is the Dirichlet trace of the solution to (2.2). $\Lambda(\sigma)$ is a compact self-adjoint operator in $\mathscr{L}(L^2_\diamond(\partial\Omega))$, with its inverse $\Lambda(\sigma)^{-1}$ being the corresponding *Dirichlet-to-Neumann* (DN) map. Notice that the roles of $\Lambda(\sigma)$ and $\Lambda(\sigma)^{-1}$ are often reversed in the literature on the inverse conductivity problem.

The purely theoretical inverse conductivity problem consists of recovering the conductivity σ when $\Lambda(\sigma)$ is given. Note that, while the ND map is a linear operator, the actual reconstruction problem is nonlinear due to the nonlinearity of the forward map $\sigma \mapsto \Lambda(\sigma)$, which relates the conductivity to the ideal boundary measurements. In the following section, we present a brief survey on the fundamental results addressing the inverse problem of determining σ from the knowledge of $\Lambda(\sigma)$.

2.2 Inverse conductivity problem

The inverse conductivity problem has inspired an impressive amount of pure and applied research in the last few decades ever since the publication of [21] by A. Calderón. To depict the nature of the problem, we analyze in this section the characteristic conditions proposed by Hadamard: the unique existence and the stability.

There have been numerous results addressing and (partially) solving the problem of uniqueness, at least in the limiting case of infinite-dimensional boundary data. Global uniqueness, that is, the injectivity of the map $\sigma \mapsto \Lambda(\sigma)$, was first shown under certain regularity assumptions on the (isotropic) conductivity σ in [93] for $d \geq 3$, and in [75] for $d = 2$. More recent results in two dimensions have substantially relaxed the assumptions on σ to measurable conductivities [8], later further generalized in [7, 76]. For dimensions $d \geq 3$, on the other hand, higher regularity is still required for both the conductivity and the domain boundary [18, 22, 39, 79]. The uniqueness results for $d > 2$ mainly follow from Calderón's work in that they construct special "complex geometric optics" solutions, essentially relating the boundary data to the Fourier transform of the conductivity. The two-dimensional results are more closely related to complex analysis and the $\bar{\partial}$, i.e. D-bar, operator. Note that for anisotropic conductivities the inverse conductivity problem is not uniquely solvable [9, 65, 92]. Recent works have also concentrated on problems with limited data, that is, current and voltage measurements available only on a subset of the boundary; see, e.g., [58, 62].

The practical problem, however, lies with the stability condition, namely the continuous dependence of the unknown σ on the data $\Lambda(\sigma)$. In fact, without accurate prior information about the conductivity, the inverse problem $\Lambda(\sigma) \mapsto \sigma$ is extremely unstable in the presence of noise, with the situation compounded in practical cases by the fact that the measurements are discrete and often available only on parts of the boundary. However, even in the purely theoretical case with infinite-dimensional data, it has been shown that such continuous dependence does not hold in general [3]. Only under sufficient smoothness constraints on the conductivity, it is possible to obtain a logarithmic type stability estimate between the topologies of $\mathscr{L}(H^{-1/2}(\partial\Omega), H^{1/2}(\partial\Omega))$ and $L^\infty(\Omega)$ [3, 11]. For a recent review of stability issues in EIT see [4, 95].

Finally, there also exist a few uniqueness and stability results for finite-dimensional boundary measurements, assuming also a finite-dimensional parametrization for the unknown conductivity. See, e.g., [1, 2] for such results employing the *continuum model* and [45] for the *complete electrode model*.

2.3 Complete electrode model

In real-life measurements with electrodes, one can only control the net currents and measure the corresponding potentials on some electrodes E_m, for $m = 1, \ldots, M$. Moreover, an electrochemical effect between an electrode and the object causes the formation of a thin and highly resistive layer at each electrode-object interface, usually characterized by a contact resistance $z_m > 0$.

The conductivity equation (2.1) combined with the contact resistance effect and the boundary conditions for the current density and electric potential on and off the electrodes leads to the following boundary value problem, known as the *complete electrode model* (CEM):

$$\begin{aligned} &\nabla \cdot (\sigma \nabla u) = 0 && \text{in } \Omega, \\ &\nu \cdot \sigma \nabla u = 0 && \text{on } \partial\Omega \setminus \overline{E}, \\ &u + z_m \nu \cdot \sigma \nabla u = U_m && \text{on } E_m, \quad m = 1, \ldots, M, \\ &\int_{E_m} \nu \cdot \sigma \nabla u \, \mathrm{d}S = I_m, && m = 1, \ldots, M. \end{aligned} \tag{2.4}$$

Here I_m and U_m define the net current and the electrode potential on the mth electrode, and $\overline{E}$ is the union of all electrodes. The isotropic conductivity distribution σ, describing the electric properties of Ω, is still assumed to belong to $L^\infty_+(\Omega)$ (cf. (2.3)).

The existence and uniqueness for the model (2.4) have been established in [89]. More precisely, for any given $I = \{I_m\}_{m=1}^M \in \mathbb{R}^M_\diamond$, there is a unique solution $(u, U) \in H^1(\Omega) \oplus \mathbb{R}^M_\diamond$, where $\mathbb{R}^M_\diamond$ denotes the mean-free subspace of $\mathbb{R}^M$. In Publications III and IV we adopt CEM, since it has been shown to be the mathematical model that most accurately reproduces real-life EIT measurements [25]. The CEM can actually be seen as a Galerkin approximation of the continuum model forward problem [52]; in fact, one can obtain the forward solutions for both the CM and the CEM by using different function spaces for the same variational formulation.

Smoothened CEM

The *smoothened* CEM was introduced in [54] to overcome the problem of limited regularity of the electromagnetic potential arising from the discontinuous Robin boundary condition in the standard CEM. The CEM traditionally assumes that contact conductances (the reciprocals of contact resistances) are constant on all electrodes and vanish in the gaps between them. This discontinuous Robin boundary condition limits the regularity of the electromagnetic potential to less than two square-integrable weak derivatives, hence deteriorating the convergence of, e.g., higher order *finite element method* (FEM).

It was shown in [54] that, by modeling the contact conductance as a *smooth* function over the whole object boundary, higher Sobolev regularity can be achieved for the forward solution and, as a result, faster convergence for some *finite element* (FE) forward solvers is obtained. This represents a major advantage especially for iterative algorithms that require repetitive and accurate solutions of the forward problem, as well as for the computation of certain quantities derived from forward solutions and needed when computing derivatives of electrode measurements with respect to geometric parameters (cf. Publication I). According to numerical tests, the smoothened version has the potential to be computationally more efficient than the standard CEM, with comparable accuracy for modeling electrode measurements. We do not verify these advantageous numerical properties of the smoothened CEM in this thesis but settle for referring to [54] for more information.

In the smoothened CEM, the *contact conductance* between the electrodes and the imaged object Ω is interpreted as a single function $\zeta \in L^\infty(\partial\Omega)$ such that

$$\zeta \geq 0, \qquad \zeta_{\partial\Omega\setminus\overline{E}} \equiv 0, \qquad \zeta|_{E_m} \not\equiv 0 \tag{2.5}$$

for all $m = 1, \ldots, M$ in the topology of $L^\infty(\partial\Omega)$. This means that the contact conductance cannot be negative, it vanishes outside the electrode patches, and on each electrode there must be a region of nonzero measure where it is positive, hence allowing current to flow.

Under these assumptions the electromagnetic potential u inside Ω and the piecewise constant electrode potential U weakly satisfy [54]

$$\begin{aligned} &\nabla \cdot (\sigma \nabla u) = 0 && \text{in } \Omega, \\ &\nu \cdot \sigma \nabla u = \zeta(U - u) && \text{on } \partial\Omega, \\ &\int_{E_m} \nu \cdot \sigma \nabla u \, \mathrm{d}S = I_m, && m = 1, \ldots, M. \end{aligned} \tag{2.6}$$

The forward problem of the standard CEM (2.4) can be easily derived from (2.6) if one constrains ζ to be constant on each electrode and defines the contact resistance on the mth electrode as $z_m := (1/\zeta)|_{E_m}$, $m = 1, \ldots, M$. As for the standard CEM, also the forward problem (2.6) for the smoothened version is uniquely solvable up to a ground level of potential [54].

2.4 Applications to stroke detection

The development of EIT for brain imaging has been relatively limited heretofore. The first published impedance scanning system appeared in the work of Benabid et al in 1978 [12], and in 1987, Holder proposed EIT as a novel means for imaging conductivity changes in the brain [51].

Although EIT for brain imaging has not yet been included into routine clinical use, considerable improvements have occurred over the past

decades in several areas, particularly in stroke detection and classification. It should be noted, however, that implementing EIT for brain imaging comprises a particularly difficult problem, since the brain is encased by a conductive covering, the *cerebrospinal fluid* (CSF), two layers with high resistivity, the *pia mater* and the *skull*, and finally the *scalp*, which has a moderate resistivity.

The ultimate goal in stroke detection by EIT is to be able to reconstruct an image of the conductivity distribution (or some partial information about it) from measurements performed with electrodes attached to the scalp.

Discretization and FEM

To practically solve the inverse problem, the capability to (numerically) solve the forward problem is typically required. In some simple cases, such as in a circular geometry with homogeneous conductivity distributions, an analytical solution for the forward problem with the continuum model can be found [81, 82]. However, in most realistic settings this is not the case, and one must necessarily resort to numerical methods. The FEM is one of the most feasible techniques for solving partial differential equations in complex geometries and with non-trivial boundary conditions [16, 26].

The basic idea in FEM is to decompose the (three-dimensional) domain into a finite number of *elements* (usually tetrahedra), and on each element the unknown potential is represented by a polynomial of a finite order. The FE discretization of the forward model is then derived from the variational formulation of the problem, and it converges to the exact solution as the number of elements becomes higher (under certain geometric assumptions) or as the order of the polynomial is increased [90].

In the following, the fundamentals of the FEM for the complete electrode model are presented, but we refer to [96] for further details. The FE approximation u^h of the solution u to (2.4) over an approximate FE mesh $\Omega_h \approx \Omega$ can be written in the form

$$u^h = \sum_{i=1}^{N} u_i \varphi_i, \tag{2.7}$$

where φ_i are the employed FE basis functions, N indicates their number, and u_i are the coefficients that are to be determined. In this work, piecewise linear basis functions are employed, which means that N coincides with the number of nodes in the FE mesh. The electrode voltages U on the M electrodes are approximated as

$$U^h = \sum_{j=1}^{M-1} U_j \eta_j, \tag{2.8}$$

with $\eta_1 = (1, -1, 0, \ldots, 0)$, $\eta_2 = (1, 0, -1, \ldots, 0)$, $\ldots$, $\eta_{M-1} = (1, 0, \ldots, -1)$.

This choice ensures that $\sum_{m=1}^{M} U_m = 0$, which corresponds to a certain systematic way of choosing the ground level of potential. In the same fashion as in (2.7), U_j represent the to-be-determined coefficients.

In [89] it has been shown that the variational formulation of (2.4) is to find $(u, U) \in H^1(\Omega) \oplus \mathbb{R}^M_\diamond$ such that

$$\mathcal{B}\big((u,U),(v,V)\big) = \sum_{m=1}^{M} I_m V_m \tag{2.9}$$

for all $v \in H^1(\Omega)$ and $V \in \mathbb{R}^M_\diamond$. Here the bilinear form $\mathcal{B}$ is defined as

$$\mathcal{B}\big((u,U),(v,V)\big) = \int_\Omega \sigma \nabla u \cdot \nabla v \, dx + \sum_{m=1}^{M} \frac{1}{z_m} \int_{E_m} (u - U_m)(v - V_m) \, dS. \tag{2.10}$$

Applying the basic theory of finite elements [16] and plugging the FEM basis functions from (2.7) and (2.8) in the variational formulation (2.10), a matrix equation for defining the unknown coefficients can be straightforwardly constructed

$$Sb = g. \tag{2.11}$$

Here, $b = (u, U)^T \in \mathbb{R}^{N+M-1}$ contains the coefficients $u = [u_i]_{i=1}^N$ and $U = [U_i]_{j=1}^{M-1}$ that are to be determined, $S \in \mathbb{R}^{(N+M-1)\times(N+M-1)}$ is a sparse block matrix of the form

$$S = \begin{pmatrix} S_1 & S_2 \\ S_2^T & S_3 \end{pmatrix}, \tag{2.12}$$

and the data vector g is given as

$$g = \begin{pmatrix} \mathbf{0} \\ \tilde{I} \end{pmatrix}, \tag{2.13}$$

with $\mathbf{0} = (0, \ldots, 0)^T \in \mathbb{R}^N$ and $\tilde{I} = (I_1 - I_2, I_1 - I_3, \ldots, I_1 - I_M)^T \in \mathbb{R}^{M-1}$. To be more precise, the blocks in (2.12) are defined as follows:

$$\begin{aligned}
(S_1)_{i,j} &= \int_\Omega \sigma \nabla \varphi_i \cdot \nabla \varphi_j \, dx + \sum_{m=1}^{M} \frac{1}{z_m} \int_{E_m} \varphi_i \varphi_j \, dS, \\
&\qquad i, j = 1, 2, \ldots, N, \\
(S_2)_{i,j} &= -\left(\frac{1}{z_1} \int_{E_1} \varphi_i \, dS - \frac{1}{z_{j+1}} \int_{E_{j+1}} \varphi_i \, dS \right), \\
&\qquad i = 1, 2, \ldots, N, \quad j = 1, 2, \ldots, M-1, \\
(S_3)_{i,j} &= \sum_{m=1}^{M} \frac{1}{z_m} \int_{E_m} (\eta_i)_m (\eta_j)_m \, dS \\
&= \begin{cases} \frac{|E_1|}{z_1}, & i \neq j \\ \frac{|E_1|}{z_1} + \frac{|E_{j+1}|}{z_{j+1}} & i = j \end{cases}, \quad i, j = 1, 2, \ldots, M-1.
\end{aligned}$$

The very same basic approach can be used for the discretization of the smoothened CEM and the Fréchet derivatives used in Publications I and IV. See [54, 69, 98] for more details.

In all reported numerical tests, the employed current patterns are such that a fixed electrode drives the current into the examined object, and it is let out in turns through the other electrodes. This is not the only, or arguably the most optimal, choice, but it is anyway used often in practice (cf., e.g., [29, 43]).

Mesh generation for the head model

The construction of the parametrized head model is extensively explained in Publications I, III and IV. However, for completeness, we present here some details about the mesh generation and the insertion of the electrodes onto the surface mesh.

To generate a head sample in our computational framework, one first needs a parametrization of a (three-layer) head, provided by the *principal component model* in Publication I. The employed model covers the upper part of the human head, sometimes referred to as the portion above the *nasion-to-inion* line. The number of anatomical layers as well as the number of the to-be-inserted electrodes and their angular positions (i.e. the polar and azimuthal coordinates of their centers) can be tuned depending on the application in hand.

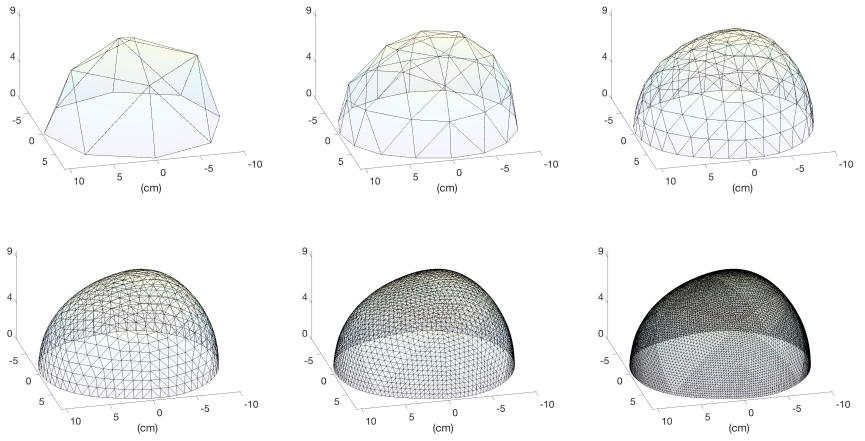

Figure 2.1. A spherical mesh is deformed $k = 6$ times to create the head surface mesh. The unit of length is centimeter.

The initial surface mesh along the exterior boundary of the considered head parametrization is constructed by subdividing k times a coarse surface partition consisting of four triangles, where $k \in \mathbb{N}$ can be tuned according to the level of precision that is aimed to be achieved. The initial surface triangulation is based on a spherical mesh, deformed to fit the

head shape parametrization (Figure 2.1).

Each electrode E_m is inserted onto the surface mesh via the workflow illustrated in Figure 2.2. We first find the surface triangles within a fixed radial distance R from an electrode center x_m, with R larger than the corresponding electrode radius R_m. The nodes in the selected patch are then projected onto the tangent plane at x_m. For further details on the projection and the exact definition of the electrodes we refer to Publication I. The actual electrode boundaries are inserted on the two-dimensional mesh in the tangent plane, and a dense mesh for the resulting polygonal domain is generated using the *Triangle* software [86]. Subsequently, the newly generated dense mesh containing the electrode boundary is re-attached to the surface mesh by utilizing a local third order polynomial representation of the surface.

After inserting all M electrodes, the process is completed by generating a tetrahedral partition for the whole volume by *TetGen* [87] starting from the formed surface mesh.

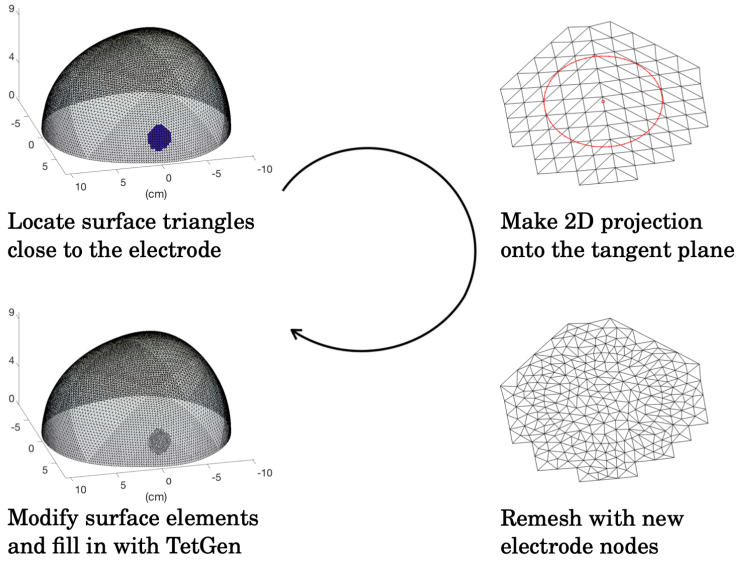

Figure 2.2. Workflow for inserting the electrodes on the boundary of the mesh. See text for more details.

For the three-layer model adopted in Publications III and IV, the boundaries of the layers are taken appropriately into account when generating three initial surface meshes; see Figure 2.3. The electrodes are then inserted onto the outermost mesh, i.e. the one corresponding to the scalp layer. The process is once again completed with the generation of a tetrahedral mesh, obeying the layer boundaries.

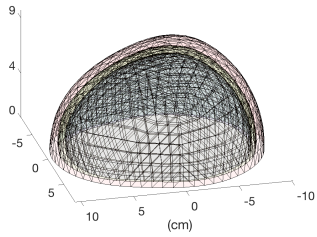

Figure 2.3. Initial (refined) surface meshes for a three-layer head model.

3. Computational approaches

Reconstruction methods for EIT can be devised according to the level of information one aims to retrieve when solving the inverse conductivity problem. In this thesis we consider the reconstruction problem using three different approaches that are presented in the following sections.

Those reconstruction methods that produce a full image of the conductivity distribution inside the examined object can be divided into iterative and direct algorithms. An iterative method generates a sequence of approximations for the unknown parameter(s) of interest, with the algorithm terminating when some pre-selected stopping criterion is satisfied [24, 68, 97, 98]. Conversely, direct reconstruction algorithms usually derive from constructive proofs, such as the widely employed $\bar{\partial}$-method [88] that provides a numerical implementation of Nachman's uniqueness proof in two dimensions [75]. A more detailed survey on this broad topic can be found in the review articles [13, 23] and the references therein. In this thesis we employ iterative methods when aiming for full conductivity reconstructions.

When considering easier problems (for instance with more prior information) one can resort to inclusion detection methods or pure classification techniques that come in handy due to their easy and fast applicability.

3.1 Iterative methods

Let us assume, for the sake of simplicity, that the conductivity σ inside our domain Ω is the only parameter to be reconstructed, and let us denote by $y \in Y$ the available boundary data (measurement), by $X = L^{\infty}_{+}(\Omega)$ the appropriate function space for σ, and by $F : X \to Y$ the problem-dependent *forward operator*.

We consider the often employed approach of finding a solution σ that minimizes a least-squares functional

$$\Phi(\sigma) = \frac{1}{2} \left\| F(\sigma) - y \right\|_Y^2 \tag{3.1}$$

accompanied by suitable regularization that reflects our prior information on the conductivity. There are multiple ways to form the regularized cost functional in (3.1). Here we present the Bayesian approach along the lines of [60, 91]; for the so-called regularization theory, see, e.g., [31]. We consider a discretized version of the conductivity $\sigma \in \mathbb{R}^N$ and a discretized/discrete measurement $F(\sigma) \in \mathbb{R}^k$, corrupted by additive noise

$$y = F(\sigma) + \eta, \tag{3.2}$$

where $\eta \in \mathbb{R}^k$ is a zero-mean Gaussian random variable with a covariance matrix $\Gamma_\eta \in \mathbb{R}^{k\times k}$. For other noise models we refer to [60]. Assuming that the noise η and the parameter σ are independent, the likelihood, i.e. the probability density of the measurement given the parameter, is also Gaussian with the same covariance Γ_η and with its mean shifted by $F(\sigma)$. The resulting probability density function has the form

$$p(y|\sigma) \propto \exp\Big(-\frac{1}{2}\big(y - F(\sigma)\big)^T \Gamma_\eta^{-1} \big(y - F(\sigma)\big)\Big),$$

where the factor $((2\pi)^k \det(\Gamma_\eta))^{-1/2}$ has been omitted since it does not depend on σ. In our analysis, the a priori information is given a density of the form

$$p(\sigma) \propto \exp\big(-\, a\, R(\sigma)\big), \tag{3.3}$$

where $a > 0$ is a free parameter and R is a penalty function describing the expected behaviour of σ. From Bayes' formula, we then get the posterior density

$$\begin{aligned} p(\sigma|y) &\propto p(y|\sigma)p(\sigma) \\ &\propto \exp\Big(-\frac{1}{2}\big(y - F(\sigma)\big)^T \Gamma_\eta^{-1} \big(y - F(\sigma)\big) - a\, R(\sigma)\Big), \end{aligned} \tag{3.4}$$

where we have again neglected the multiplicative terms independent of σ.

Solving an inverse problem in the Bayesian framework requires addressing the following matters: (i) devise a prior probability density $p(\sigma)$ that reflects the qualitative information on the unknown σ, (ii) find the likelihood function $p(y|\sigma)$ according to the problem-specific mathematical model, and (iii) develop and/or apply methods to explore the posterior probability density $p(\sigma|y)$.

Since in practical settings the dimension of the to-be-reconstructed parameter is usually relatively high, thus preventing a direct visualization of the posterior distribution, one typically needs to resort to point estimates for practical purposes. One of the statistical estimates which is most commonly used is the *maximum a posteriori* (MAP)

$$\sigma_{\text{MAP}} = \arg\max_{\sigma\in\mathbb{R}^N} p(\sigma|y),$$

provided that such a maximizer exists (and even if it exists, it may not be unique). Computing a MAP estimate for (3.4) corresponds to finding a minimizer for a nonlinear Tikhonov-type functional of the form

$$\Phi(\sigma) = \frac{1}{2}\big(y - F(\sigma)\big)^T \Gamma_\eta^{-1}\big(y - F(\sigma)\big) + a\, R(\sigma), \tag{3.5}$$

which is usually done by using iterative methods.

In Publication I and IV there are more than one unknown parameters, namely the conductivity distribution, the contact resistances (or conductances), the electrode positions and the shape parameters defining the head geometry. As an example, in the case of two independent parameters that need to be reconstructed (here the conductivity σ and the contact resistances z), the Tikhonov functional (3.5) should be modified into

$$\Phi(\sigma, z) = \frac{1}{2}\big(y - F(\sigma, z)\big)^T \Gamma_\eta^{-1}\big(y - F(\sigma, z)\big) + a_1\, R_1(\sigma) + a_2\, R_2(z), \tag{3.6}$$

where the corresponding prior information has been accounted for via appropriate choices for the penalty functions R_1 and R_2, and the free parameters a_1 and a_2.

Choice of priors

Selecting a suitable prior density (3.3) corresponds to translating the qualitative prior knowledge on the unknowns into a quantitative form. In statistical inverse problems the most common probability densities are arguably Gaussian, as they are computationally easy to handle and they may also give good approximations even for inherently non-Gaussian distributions. In our setting, the choice of prior corresponds to selecting a suitable function $R(\sigma)$ in (3.3). Choosing

$$R(\sigma) = \frac{1}{2a}(\sigma - \sigma_0)^T \Gamma_\sigma^{-1}(\sigma - \sigma_0) \tag{3.7}$$

gives the parameter of interest σ a Gaussian prior density with the mean $\sigma_0 \in \mathbb{R}^N$ and the positive definite covariance $\Gamma_\sigma \in \mathbb{R}^{N\times N}$.

The choice of the covariance matrix Γ_σ can be handled in many ways, but it should always be related to prior or expert information on the studied measurement setup. In the numerical studies of Publication I this choice depends on the character of the parameter in question. As an example, the penalty function $R(\theta)$ associated to the prior density for the electrode polar angle is defined by

$$\Gamma_\theta = \gamma^2 \mathbb{I}, \tag{3.8}$$

where $\mathbb{I} \in \mathbb{R}^{M\times M}$ is the identity matrix and γ determines the standard deviation in the polar direction; γ is chosen so that it reflects typical errors in the positioning of the electrodes. On the other hand, it is natural to assume that there is some correlation between the values of the conductivity

evaluated at nodes lying close to one another in the utilized FE mesh. To this end, we introduce the distance-dependent covariance matrix

$$(\Gamma_\sigma)_{i,j} = \gamma^2 \exp\left(- \frac{\|x_i - x_j\|^2}{2l^2} \right), \qquad i,j = 1,\ldots,N, \tag{3.9}$$

where $\gamma > 0$ is the pointwise standard deviation, $x_i, x_j \in \mathbb{R}^3$ are coordinates of the FE nodes in the head mesh, and $l > 0$ is the correlation length.

In Publication IV we aim to incorporate a different qualitative feature in the prior for the conductivity: the imaged object is assumed to contain well localized inclusions with approximately constant conductivity levels. In other words, this characterization means that the conductivity is expected to exhibit local jumps in an otherwise homogeneous background. In such cases, one can consider a non-Gaussian prior density with the function R being a discretized version of a regularizer

$$\mathcal{R}(\sigma) := \int_\Omega r\big(|\nabla\sigma(x)|\big)\, dx, \tag{3.10}$$

where $r : \mathbb{R}_+ \to \mathbb{R}_+$ is a suitable continuously differentiable, monotonically increasing function [5]. An example of such a function is provided by the smoothened *total variation* (TV) prior [80] for which

$$r(t) = \sqrt{T + t^2} \approx |t|, \tag{3.11}$$

where $T > 0$ is a small parameter that ensures the differentiability of r. Other suitable choices are, e.g., a *Perona-Malik* or a smoothened TV^q prior [50].

Modeling errors

We mentioned in Section 2.2 the instability of the inverse problem of EIT with respect to measurement and modeling errors, arising, e.g., from uncertainty about model parameters such as the electrode locations, the contact resistances, and the shape of the imaged object. The simplest way to tackle inaccurate geometric modeling is *difference imaging* [10], that is, electrode measurements are performed at two separate times with the aim of reconstructing the corresponding difference in the conductivity. The obvious advantage is that the modeling errors partially cancel out, but unfortunately reference measurements are not available in many EIT applications, such as stroke detection in the case of emergency.

If we limit ourselves to *absolute imaging*, where EIT measurements are available at a single time frame and at a single frequency, there exist a few algorithms for handling geometric uncertainties. In the one introduced in [66, 67] mainly for two-dimensional EIT, reconstruction of anisotropic conductivities is considered to compensate for the domain mismodeling. Moreover, [53] built a polynomial surrogate for the dependence

of the boundary measurements of EIT on several unknowns, including the parametrized measurement geometry, and employed this surrogate in straightforward Tikhonov regularization in two spatial dimensions.

In [14, 29, 59, 98], the estimation of certain model parameters is included as a part of iterative algorithms designed originally for mere conductivity reconstruction; in these works the dimensions of the to-be-reconstructed parameters are reasonably low and the computation of the corresponding derivatives relatively cheap, which means that the efficiency of the considered algorithms does not considerably suffer from the incorporation of the extra unknowns. In the setting of head imaging, it is also possible to develop and utilize differentiability results that are well-suited for numerical applications. It is well-established that the electrode potential pattern U is Fréchet differentiable with respect to the conductivity and the contact resistances; see, e.g., [33, 68, 98]. Certain differentiability results have also been previously developed for the dependence of the electrode measurements on the electrode locations and the shape parameters defining the object boundary [27, 28]. These results and ideas are employed in Publication I for reconstructing the head shape and the electrode locations at the same time as the conductivity inside the examined head (without the skull layer). To be quite precise, the differentiation formulas introduced in [27, 28] are only employed for computing derivatives with respect to the electrode locations, while the derivatives with respect to the head shape are approximated via central differences.

Finally, the so-called *approximation error* approach introduced in general by [60] and for EIT in [77, 78] is used for recovering from geometric mismodeling in Publication IV. In the approximation error method, the modeling error is represented as an additive stochastic noise term whose (second order) statistics are approximated via simulations. In our work these statistics are estimated in advance based on extensive simulations and prior knowledge on the unknown parameters; subsequently, the approximation error noise is combined with the actual measurement noise and accounted for within the Bayesian inversion paradigm. The actual inversion is performed by reconstructing the deviation of the conductivity (inside the examined head) from an expected conductivity using an "average" head model as a fixed reference domain. The studies in Publication IV account for uncertainties in head and skull shapes, electrode positions and contact resistances.

Minimization schemes

A minimization scheme for the functional in (3.5) requires solving the necessary condition $\nabla\Phi(\sigma) = 0$, which leads to different methods depending on the required accuracy and the nature of the penalty term $R(\sigma)$ in (3.5).

If $R(\sigma)$ is quadratic (as in Publication I), the minimization of Φ corre-

sponds to a nonlinear least square problem, efficiently solvable with a Gauss–Newton type algorithm. Resorting to FEM, we evaluate approximations for the forward solution $F(\sigma^{(l)})$ and the Jacobian $J_\sigma^{(l)} = J_\sigma^F(\sigma^{(l)})$ of the map $\sigma \mapsto F(\sigma)$ at a given point $\sigma^{(l)}$. We then approximate the forward solution around $\sigma^{(l)}$ by its linearization

$$F(\sigma) \approx F(\sigma^{(l)}) + J_\sigma^{(l)}(\sigma - \sigma^{(l)}),$$

and use it to write the to-be-minimized functional (3.5) in an approximate form

$$\Phi^{(l)}(\sigma) := \frac{1}{2}(y^{(l)} - J_\sigma^{(l)}\sigma)^T \Gamma_\eta^{-1}(y^{(l)} - J_\sigma^{(l)}\sigma) + a\,R(\sigma),$$

where $y^{(l)} = y - F(\sigma^{(l)}) + J_\sigma^{(l)}\sigma^{(l)}$. The condition $\nabla\Phi^{(l)}(\sigma) = 0$ is then equivalent to the equation

$$(J_\sigma^{(l)})^T \Gamma_\eta^{-1} J_\sigma^{(l)}\sigma + a(\nabla R)(\sigma) = (J_\sigma^{(l)})^T \Gamma_\eta^{-1} y^{(l)}. \tag{3.12}$$

In the quadratic case (3.7), we have $(\nabla R)(\sigma) = \Gamma_\sigma^{-1}(\sigma - \sigma_0)$ and (3.12) thus becomes

$$A^T A\, d^{(l)} = A^T \begin{bmatrix} L_\eta(y - F(\sigma^{(l)})) \\ \sqrt{a}L_\sigma(\sigma_0 - \sigma^{(l)}) \end{bmatrix}, \qquad A = \begin{bmatrix} L_\eta J_\sigma^{(l)} \\ \sqrt{a}L_\sigma \end{bmatrix}, \tag{3.13}$$

with $L_\eta^T L_\eta = \Gamma_\eta^{-1}$ and $L_\sigma^T L_\sigma = \Gamma_\sigma^{-1}$ being Cholesky factorizations of the inverse covariance matrices, and $d^{(l)} = \sigma - \sigma^{(l)}$. In other words, (3.12) becomes a standard quadratic Tikhonov functional, and (3.13) is the normal equation corresponding to the associated least squares problem. Now $\sigma^{(l+1)}$ can be defined based on (3.13), and the iteration continued until the chosen stopping criterion is satisfied.

When several parameters are included in the estimation process, the derivatives of the electrode potentials with respect to each of them must be approximated, and the corresponding Jacobians and prior covariance matrices must be appropriately incorporated in (3.13). More specifically, the Jacobian matrices can be computed explicitly by sampling their rows using suitable variational formulations [27, 54, 55, 98].

If $R(\sigma)$ originates from a regularizer of the form (3.10) (as in Publication IV), the *lagged diffusivity* method [99] can be used in connection to linear forward operators $F(\sigma) = F\sigma$. The algorithm is based on the fact that the contribution of the penalty term $R(\sigma)$ to the necessary condition for a minimizer of (3.5) can be written as $(\nabla R)(\sigma) = H(\sigma)\sigma$, where H is a parameter-dependent regularization matrix defined via

$$H_{i,j}(\sigma) := \int_\Omega \frac{r'(|\nabla\sigma(x)|)}{|\nabla\sigma(x)|}\nabla\varphi_i(x)\cdot\nabla\varphi_j(x)\,dx, \qquad i,j = 1,\ldots,N, \tag{3.14}$$

with the help of the employed piecewise linear FE basis functions φ_i. The condition $\nabla\Phi(\sigma) = 0$ is then equivalent to

$$A^T A\sigma = A^T \begin{bmatrix} L_\eta y \\ 0 \end{bmatrix}, \qquad A = \begin{bmatrix} L_\eta F \\ \sqrt{a} L_\sigma \end{bmatrix}, \tag{3.15}$$

where $L_\eta^T L_\eta = \Gamma_\eta^{-1}$ and $L_\sigma^T L_\sigma = H(\sigma)$ are again Cholesky factorizations[1]. The basic idea is then to solve (3.15) iteratively, with L_σ always evaluated at the previous estimate for σ, thus making (3.15) a linear equation for the next iterate.

In case of nonlinear forward operators, *combined algorithms* can be utilized as in [43], where the authors combine sequential linearizations of the forward map in a Gauss–Newton iteration with lagged diffusivity steps for the linearized inverse problems with an edge-promoting penalty term. This is also the key idea for the optimization approach in Publication IV.

3.2 Inclusion detection methods

The goal of inclusion detection methods is retrieving information on an unknown conductivity perturbation in a known background. Such a setting is considered in numerous imaging applications, including detecting inhomogenitites in some building material and, within medical applications, distinguishing anomalies (cancerous tissue or hemorrhages) from a (known) healthy background.

Among the first of such methodologies was the *factorization method*, introduced for inverse scattering by Kirsch [63] and modified for EIT by Brühl and Hanke [20, 19]. The method is applicable in settings where the conductivity levels of the inclusions are either higher or lower than the background [35, 37, 44, 52, 64]. As another example, the *enclosure method* of Ikehata [56, 57, 15] aims to recover the convex hull of an inclusion, based on the asymptotics of a certain indicator function.

The approach we consider in this work is the *monotonicity method*, originating from and numerically tested in a paper of Tamburrino and Rubinacci [94], and rigorously proven to function later on by Harrach and Ullrich [44, 46, 47] with the help of the theory of localized potentials [36]. Although the monotonicity method is closely related to the factorization method, it is in addition capable to simultaneously reconstruct both conductive and insulating inclusions, and it also has a natural interpretation for electrode measurements [33, 47].

[1]The positive definiteness of $H(\sigma)$ is ensured by including suitable boundary conditions or shifting its spectrum slightly right away from the origin.

Monotonicity method

The monotonicity method exploits the physically intuitive monotonicity principles for the Neumann-to-Dirichlet map Λ

$$\sigma \leq \tau \quad \text{implies} \quad \Lambda(\sigma) \geq \Lambda(\tau), \tag{3.16}$$

where the latter inequality is to be understood in the sense of positive definiteness. In other words, the power needed for maintaining any (direct) boundary current pattern increases if the conductivity inside the imaged object decreases. In mathematical terms, current-voltage measurements in EIT can be partially ordered with respect to the definiteness of the associated self-adjoint Neumann-to-Dirichlet operators, so that an almost everywhere larger conductivity leads to less positive definite current-voltage measurements, and vice versa. A converse of this monotonicity relation can be used to solve the inclusion detection problem in EIT (also referred to as *shape reconstruction*) by simply comparing the acquired measurements to those related to carefully chosen (computational) test inclusions. The basic ideas of the method are described in some more detail in what follows; we refer to [46, 47] for more information.

Let Ω contain inclusions in which the conductivity σ differs from an otherwise known background conductivity σ_0, which is required to carry a suitable unique continuation property. For simplicity, let us consider the (unrealistic) setting where continuum measurements are available on the complete boundary $\partial\Omega$. Under certain geometric assumptions, the inclusion shape, defined as the set $\mathrm{supp}(\sigma - \sigma_0)$, can be reconstructed by so-called *monotonicity tests* that compare $\Lambda(\sigma)$ to ND operators $\Lambda(\tau)$, defined by certain test conductivities τ, in the sense of positive definiteness. Moreover, the test ND operators $\Lambda(\tau)$ can be replaced, without losing any information, by their linear approximations using the Fréchet derivative $\Lambda'(\sigma_0)$ of $\Lambda(\sigma)$ at the background conductivity.

For a better understanding of the monotonicity method, let us state its results in two example configurations that correspond to two frequently considered special cases: the *definite case* (1), in which all inclusions have a higher (or lower) conductivity than the background, and the *indefinite case* (2), where the conductivity may differ in both directions from the background value. In both examples, the considered conductivity values are bounded away from zero and infinity. However, the main result of Publication II shows how to also handle *extreme inclusions*, which correspond to some parts of the domain being either perfectly conducting ($\sigma = \infty$) or perfectly insulating ($\sigma = 0$).

Examples with $\sigma_0 = 1$ [46]:

1. Let $\sigma = 1 + \chi_D$ where D is open, with χ_D being its characteristic function, and $\overline{D} \subset \Omega$ has a connected complement. Then, for every

open ball $B \subset D$

$$B \subseteq D \quad \text{if and only if} \quad \Lambda(1+\chi_B) \geq \Lambda(\sigma)$$

$$\text{if and only if} \quad \Lambda(1) + \frac{1}{2}\Lambda'(1)\chi_B \geq \Lambda(\sigma).$$

2. Let $\sigma = 1 + \chi_{D^+} - \frac{1}{2}\chi_{D^-}$ where D^+, $D^- \subseteq \Omega$ are open, $\overline{D^+} \cap \overline{D^-} = \emptyset$, and $\overline{D^+} \cup \overline{D^-} \subset \Omega$ has a connected complement. Then, for every closed $C \subset \Omega$ with connected complement

$$D^+ \cup D^- \subseteq C$$

$$\text{if and only if} \quad \Lambda(1+\chi_C) \leq \Lambda(\sigma) \leq \Lambda\Big(1 - \frac{1}{2}\chi_C\Big)$$

$$\text{if and only if} \quad \Lambda(1) + \Lambda'(1)\chi_C \leq \Lambda(\sigma) \leq \Lambda(1) - \Lambda'(1)\chi_C.$$

Note that the constant conductivity values inside the inclusions D, D^+ and D^- have been chosen arbitrarily. In fact, such values need not be constant, and the assumptions on the geometry of the inclusions can also be relaxed. See, e.g., [46] for more details.

The first case exemplifies that a definite inclusion D can be recovered as the union of all balls B that satisfy the monotonicity tests in (1), by either comparing ND maps for different conductivities or by using the corresponding linearized condition. The latter option may often be advantageous as it does not require solving the forward problem for multiple conductivities. The result for the indefinite case works in the opposite way: the monotonicity tests in (2) show how to deduce whether a larger set C contains the inclusions D^+ and D^-, the combination of which can eventually be obtained as the intersection of all such larger sets C.

The monotonicity method is easily applicable to practical setting since both tests (1) and (2) allow stable implementations, although the one for the definite case is considerably simpler [33, 34, 47]. Also, the presented results naturally extend to the case of partial boundary measurements [46]. More recently, the monotonicity method has also been applied to the reconstruction of piecewise constant layered conductivities [32].

3.3 Machine learning-based classification

Machine learning is a branch of artificial intelligence that utilizes methods and algorithms for the automatic creation of data models. Contrary to standard mathematical methods that execute tasks by following explicit and predefined algorithms, a machine learning model constantly "learns" from data and experience. This means that, on the one hand, it can always improve its performance by learning from newly acquired data,

but, on the other hand, predictions may not always be fully accurate and one should pay particular attention to the reliability of the results. Nevertheless, the use of such algorithms is vast among a wide variety of fields, among which are computer science, economics and medicine. Machine learning techniques can be considered particularly attractive if the studied phenomenon is not easily modellable or if traditional models are computationally unfeasible.

In recent years, machine learning has brought about advances in ill-posed and inverse problems [6, 73, 74], and, in particular, it has been successfully applied in EIT imaging [41, 42, 72, 85]. In the specific case of stroke detection, such methods can be used for classification of stroke as such but also as a support tool to improve the full image reconstructions.

There is a tremendous number of machine learning algorithms available in the literature, and it is not always clear which is the most suitable for the considered problem. Among them, *Neural Networks* (NNs) are algorithms designed to capture underlying relationships in a set of data through a process that mimics, to a certain extent, the neurological functions. In Publication III we investigate the potential of Neural Networks for *classification* of stroke. All classification tasks fall under so-called *supervised learning*, that is, they require the preparation of labeled datasets in order for the considered neural networks to learn the correlation between data and labels.

Neural Networks

A neural network is composed of a collection of connected nodes or *neurons* organized in different layers (see Figure 3.1). To put it short, each neuron receives a set of inputs (the data), which are multiplied with random weights and added to a bias value. The result is transmitted to an appropriate *activation function*, which provides the final output value that exits the neuron. Once the output is generated from the final neural net layer, a *loss function* is calculated based on the training set and the weights are adjusted to minimize the loss. Finding optimal weights is the aim of this type of classification learners.

There are countless neural network architectures available and just as many choices for the related hyperparameters. For a comprehensive review on this broad topic we refer to [70, 84]. A *Fully Connected Neural Network* (FCNN) consists of a series of layers in which all neurons have complete connections to all neurons in the previous layer, with a weight specific to each connection (Figure 3.1). These networks are very broadly applicable, since they do not require any assumptions on the features in the data. However, they can be computationally expensive in terms of memory and computation time, and also can exhibit a weaker performance than networks specifically tuned to the problem at hand.

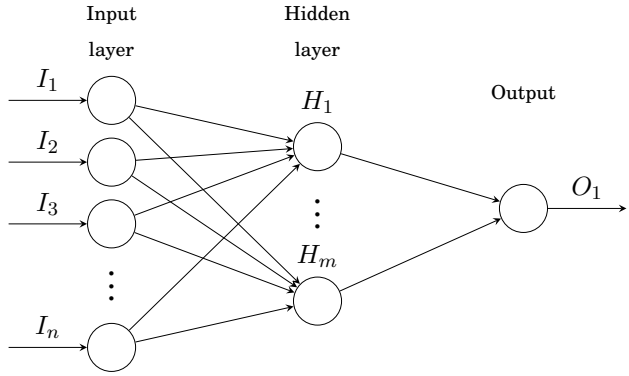

Figure 3.1. An illustration of the architecture of a FCNN, with n neurons in the input layer (n being the size of our data), m neurons in the hidden layer and one output neuron for classification purposes.

In contrast, in a layer of a *Convolutional Neural Network* (CNN) each neuron is connected to a (usually) small number of neighboring neurons in the previous layer, and the input values are multiplied with the same set of weights (see the first connections in Figure 3.2). This option usually makes sense for cases where the data are assumed to have spatial relations, with the typical application being processing image data. Compared to the computational aspects of fully connected networks, convolutional layers are relatively cheap thanks to the lower number of connections and weights, but their performance strongly depends upon underlying spatial assumptions.

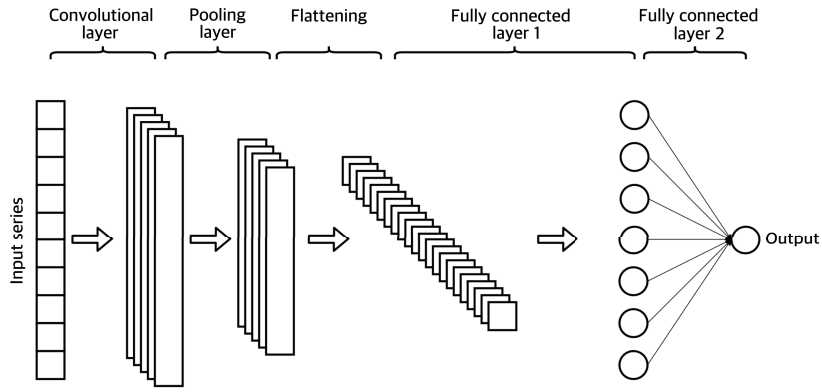

Figure 3.2. An illustration of the architecture of a CNN. The convolutional and the pooling layers are typically applied to consistently reduce the size of the problem, which is then transferred to a fully connected structure.

Defining the architecture of a neural network is in itself a difficult task, since for the choice of many hyperparameters there are no universally established criteria. A (partial) solution to this shortcoming is presented

by automatic machine learning (AutoML) algorithms, which have been designed to systematically test different models and automatically optimize the hyperparameters [48]. AutoML can be, however, extremely time consuming and computationally expensive. In the following, we report some of the most important design issues to consider when implementing a fully connected or a convolutional neural network [61].

While characterizing the general structure of a FCNN only requires the specification of the number of layers and the number of neurons in each layer, CNNs require a more thought-through process. *Convolutional layers* need to be defined with additional hyperparameters, such as the *kernels* (described by a width and a height), the number of input and output channels, and the parameters related to the convolution operation, i.e. *stride* and *padding*. Convolutional layers are used to *convolve* the inputs with different kernels and transfer the result to the next layer. *Pooling layers* typically reduce the dimensions of data by combining (according to a specified criterion) the outputs of neuron clusters from one layer into a single neuron in the next layer. Finally, *flattening* is the operation of converting the data into a one-dimensional array for inputting it to the next layer.

In addition to the network macro structure, there is a collection of other parameters and functions to be defined.

- The *activation function* defines the output of a node given a set of inputs. The modern default activation function for hidden layers is the *Rectified Linear Unit* (ReLU) activation function (denoted below by h), while for output layers a conventional choice is a sigmoid function (denoted by s)

$$h(x) = \max(0, x), \qquad s(x) = 1/(1 + e^{-x}). \tag{3.17}$$

- The *loss function* (or cost function) measures the performance of a classification model whose output is a probability value. Among the binary classification loss functions, one common choice is the *Binary Cross Entropy* (BCE) function, which defines the way in which network training penalizes for the deviations between the predicted and the true labels. If we denote by ϑ the set of weights and biases, then

$$L(\vartheta) = -\sum_j \Big(y_j \log(p_j) + (1 - y_j) \log(1 - p_j) \Big), \tag{3.18}$$

  where y_j is a binary value (0 or 1) indicating if the predicted class label is correct, and p_j is the corresponding output probability, implicitly dependent on the training data and on the set of network parameters ϑ.

- The *optimization algorithm* (or optimizer) provides the method for changing the weights and the biases to minimize the loss. Many

optimizers are based on gradient descent, a well known family of optimization algorithms requiring (only) the first order derivatives of the loss function. The corresponding general procedure for updating the weights so that the loss function can reach a (possibly local) minimum is

$$\vartheta = \vartheta - \mu \nabla_{\vartheta} L(\vartheta), \tag{3.19}$$

where $\mu > 0$ is a step size or *learning rate*.

- The *learning rate* μ is a tuning parameter that determines the step size at each iteration of the optimization algorithm while descending toward a minimum of a loss function. It can be thought as the "speed" at which a machine learning model "learns".

- When dealing with large datasets, as is usually the case, the *batch size* defines the number of samples from the training data that are propagated through the network. With small batch sizes training is faster and requires less memory, but the estimate for the gradient of the loss function is less accurate than with larger batches.

- One *epoch* corresponds to an entire dataset passing forward and backward through the neural network only once, which is usually not enough for defining the optimal weights (*underfitting*). As the number of epochs increases, the weights are updated more times and better optimality is hopefully reached. With too many epochs, however, the network tends to *overfit* to the learning data.

- In supervised machine learning, the available data set is usually divided into subsets for the training, validation and testing phases. Training is typically performed based on the *training dataset* and prediction is carried out based on the *validation dataset* at the end of each epoch. Errors for the validation dataset can be used to identify stopping criteria and to fine-tune hyperparameters. Above all, errors for the validation dataset can help to find out if the model has overfitted to the training data. Prediction against the *test dataset* is typically performed only on the final model. Another common technique for data splitting is *cross-validation*, where the initial data set is repeatedly mixed and split at the begin of each epoch into training and validation dataset.

4. Summary of results

I: Computational framework for applying electrical impedance tomography to head imaging

Publication I introduces a computational framework for applying absolute EIT to practical head imaging. The idea is to utilize the derivatives of the electrode potentials with respect to the exterior boundary shape and the electrode locations in a regularized Newton-type output least squares algorithm that simultaneously reconstructs all relevant unknowns.

To build a parametrization for the natural variations in head shapes and sizes over the human population, we employ a library of human heads and form a *principal component* model for the associated geometric variations. We also present a robust and efficient way to mesh the parametrized head model to enable fast forward solutions by FEMs. We use the smoothened CEM presented in Section 2.3 as the forward model and employ relatively dense FE meshes in order to overcome a certain instability in the computation of the Fréchet derivatives with respect to geometric parameters.

The functionality of the method is tested via numerical experiments on simulated noisy data with noise levels comparable to those reported for standard EIT systems. Each unknown parameter is assigned a Gaussian prior, and a MAP estimate is computed iteratively, as explained in Section 3.1. Our numerical experiments demonstrate that strong enough variations in the conductivity of an imaged head can be reconstructed in this manner even under moderate geometric uncertainties. Moreover, there is some evidence that mismodeling of the head shape can be partially compensated by only including the estimation of the electrode positions in a reconstruction algorithm implemented in a fixed average head geometry. The effect of the insulating skull layer is not considered in this study.

II: Monotonicity-based reconstruction of extreme inclusions in electrical impedance tomography

The main topic of this work is to generalize the monotonicity method

overviewed in Section 3.2 to allow extreme inclusions inside the domain of interest; by "extreme" we mean perfectly conducting or perfectly insulating. This is achieved by establishing suitable monotonicity principles for the ND map (cf. Section 2.1) in the presence of extreme inclusions. For this purpose, we first show that any ND map that corresponds to extreme inclusions can be reached in the natural operator topology as a limit of a sequence of standard ND maps, i.e. ones without extreme inclusions, when the conductivity coefficient decays to zero and/or grows to infinity in the appropriate parts of the domain.

Combining this result with the standard monotonicity relations for the ND maps corresponding to finite and positive conductivities, we demonstrate that both definite and indefinite inclusions can be reconstructed with the monotonicity method in the presence of extreme inclusions. In particular, our result on the indefinite case covers a wide class of inclusions: the perturbed conductivity can simultaneously have parts that are perfectly insulating and parts that are perfectly conducting, as well as other perturbed parts bounded away from zero and infinity.

Although this thesis does not implement the monotonicity method as a practical algorithm for stroke detection, the presented results pave the way for such considerations by enabling detection of inclusions under very mild assumptions on their geometry and conductivity levels.

III: Neural networks for classification of strokes in electrical impedance tomography on a 3D head model

This work applies neural networks to the detection of brain hemorrhages from simulated absolute EIT data on the 3D head model from Publication I, extended in a natural way to handle more complicated anatomical structures. To this end, we simulate large datasets that are used to train and test a fully connected and a convolutional neural network (see Section 3.3).

The training and test datasets are composed of pairs of synthetic noisy electrode measurements and a label indicating whether the data are associated with a hemorrhagic stroke or not. This classification is motivated by the assumption that detecting the presence or absence of a hemorrhage is sufficient for initiating appropriate medical treatment. The measurements are simulated with the CEM (Section 2.3) and generated by varying the conductivity distribution, the electrode positions, the measurement noise, the shape of the head, and the interior and exterior surfaces of the skull. The testing of the networks is performed on several datasets of unseen EIT data, with more complex stroke modeling (different shapes and volumes), higher levels of noise and different amounts of electrode misplacement.

Despite the use of simple neural network architectures, the obtained results are promising and motivate the testing of EIT-based classification methods on real phantoms and ultimately on human patients. In fact, our

numerical tests show that the probability of detecting a hemorrhagic stroke is reasonably high, even when the electrodes suffer from considerable misplacement and the geometric model for the head is notably inaccurate. In our experiments, a shallow fully connected neural network exhibits superior performance compared to a convolutional one.

IV: Approximation error method for imaging the human head by electrical impedance tomography

In this work we combine the principal component head model from Publications I and III with the approximation error method. The second order statistics of the approximation error are estimated by following the ideas of Publication III. To be more precise, the learning data is formed by computing simulated EIT measurements with the CEM for an ensemble of random head and skull shapes, electrode locations, contact resistances and tissue conductivities. The needed statistics are then simulated by considering the deviation of these measurements from the ones corresponding to the intended electrode positions and the mean anatomy inside the average head of the employed principal component model.

The actual inversion is performed by reconstructing the deviation of the conductivity (inside the examined head) from the expected conductivity in the average head model, accounting for both the actual measurement noise and the approximation error noise within the Bayesian paradigm (cf. Section 3.1). An edge-preferring prior density is considered for the (discretized) change in the conductivity, which means that computing a MAP estimate thus corresponds to finding a minimizer for a Tikhonov-type functional that is non-quadratic in both the discrepancy and the penalty term.

The algorithm is tested on simulated noisy data with and without including the approximation error process in the measurement model. With approximation error modeling, our algorithm produces useful information on the stroke, and it clearly outperforms reconstructions with the conventional measurement error model if the information on the measurement geometry is incomplete. These results indicate that the presented method can be a potential alternative for stroke classification in emergency care, where one would practically always lack the exact knowledge on the electrode locations and the geometry of the patient's head.

References

[1] G. S. Alberti and M. Santacesaria. Calderón's inverse problem with a finite number of measurements. In *Forum of Mathematics, Sigma*, volume 7. Cambridge University Press, 2019.

[2] G. S. Alberti and M. Santacesaria. Calderón's inverse problem with a finite number of measurements II: independent data. *Applicable Analysis*, pages 1–19, 2020.

[3] G. Alessandrini. Stable determination of conductivity by boundary measurements. *Applicable Analysis*, 27(1-3):153–172, 1988.

[4] G. Alessandrini. Open issues of stability for the inverse conductivity problem. *Journal of Inverse and Ill-Posed Problems*, 15:451–460, 2007.

[5] S. R. Arridge, M. M. Betcke, and L. Harhanen. Iterated preconditioned LSQR method for inverse problems on unstructured grids. *Inverse Problems*, 30(7):075009, 2014.

[6] S. R. Arridge, P. Maass, O. Öktem, and C.-B. Schönlieb. Solving inverse problems using data-driven models. *Acta Numerica*, 28:1–174, 2019.

[7] K. Astala, M. Lassas, and L. Päivärinta. The borderlines of invisibility and visibility in Calderón's inverse problem. *Analysis & PDE*, 9(1):43–98, 2016.

[8] K. Astala and L. Päivärinta. Calderón's inverse conductivity problem in the plane. *Annals of Mathematics*, pages 265–299, 2006.

[9] K. Astala, L. Päivärinta, and M. Lassas. Calderón's inverse problem for anisotropic conductivity in the plane. *Communications in Partial Differential Equations*, 30(1-2):207–224, 2005.

[10] D. C. Barber and B. H. Brown. Applied potential tomography. *Journal of Physics E: Scientific Instruments*, 17(9):723, 1984.

[11] J. A. Barceló, T. Barceló, and A. Ruiz. Stability of the inverse conductivity problem in the plane for less regular conductivities. *Journal of Differential Equations*, 173(2):231–270, 2001.

[12] A. L. Benabid, L. Balme, J. C. Persat, M. Belleville, J. P. Chirossel, M. Buyle-Bodin, J. de Rougemont, and C. Poupot. Electrical impedance brain scanner: principles and preliminary results of simulation. *T.-I.-T. Journal of Life Sciences*, 8(1-2):59–68, 1978.

[13] L. Borcea. Electrical impedance tomography. *Inverse Problems*, 18(6):R99–R136, 2002.

[14] A. Boyle, A. Adler, and W. R. B. Lionheart. Shape deformation in two-dimensional electrical impedance tomography. *IEEE Transactions on Medical Imaging*, 31(12):2185–2193, 2012.

[15] T. Brander, M. Kar, and M. Salo. Enclosure method for the p-Laplace equation. *Inverse Problems*, 31(4):045001, 2015.

[16] S. Brenner and R. Scott. *The mathematical theory of finite element methods*, volume 15. Springer, 2007.

[17] B. H. Brown. Electrical impedance tomography (EIT): a review. *Journal of Medical Engineering & Technology*, 27(3):97–108, 2003.

[18] R. M. Brown and R. H. Torres. Uniqueness in the inverse conductivity problem for conductivities with $3/2$ derivatives in L^p, $p > 2n$. *Journal of Fourier Analysis and Applications*, 9(6):563–574, 2003.

[19] M. Brühl. Explicit characterization of inclusions in electrical impedance tomography. *SIAM Journal on Mathematical Analysis*, 32(6):1327–1341, 2001.

[20] M. Brühl and M. Hanke. Numerical implementation of two noniterative methods for locating inclusions by impedance tomography. *Inverse Problems*, 16(4):1029, 2000.

[21] A. Calderón. On an inverse boundary value problem. *Seminar on Numerical Analysis and its Applications to Continuum Physics (Rio de Janeiro, 1980)*, pages 65–73, 1980.

[22] P. Caro and K. M. Rogers. Global uniqueness for the Calderón problem with Lipschitz conductivities. In *Forum of Mathematics, Pi*, volume 4, 2016.

[23] M. Cheney, D. Isaacson, and J. C. Newell. Electrical impedance tomography. *SIAM review*, 41(1):85–101, 1999.

[24] M. Cheney, D. Isaacson, J. C. Newell, S. Simske, and J. Goble. NOSER: An algorithm for solving the inverse conductivity problem. *International Journal of Imaging Systems and Technology*, 2(2):66–75, 1990.

[25] K.-S. Cheng, D. Isaacson, J. C. Newell, and D. G. Gisser. Electrode models for electric current computed tomography. *IEEE Transactions on Biomedical Engineering*, 36(9):918–924, 1989.

[26] P. G. Ciarlet. *The finite element method for elliptic problems*. SIAM, 2002.

[27] J. Dardé, H. Hakula, N. Hyvönen, and S. Staboulis. Fine-tuning electrode information in electrical impedance tomography. *Inverse Problems & Imaging*, 6(3):399–421, 2012.

[28] J. Dardé, N. Hyvönen, A. Seppänen, and S. Staboulis. Simultaneous reconstruction of outer boundary shape and admittivity distribution in electrical impedance tomography. *SIAM Journal on Imaging Sciences*, 6(1):176–198, 2013.

[29] J. Dardé, N. Hyvönen, A. Seppänen, and S. Staboulis. Simultaneous recovery of admittivity and body shape in electrical impedance tomography: an experimental evaluation. *Inverse Problems*, 29(8):085004, 2013.

[30] T. Dowrick, C. Blochet, and D. S. Holder. In vivo bioimpedance measurement of healthy and ischaemic rat brain: implications for stroke imaging using electrical impedance tomography. *Physiological Measurement*, 36(6):1273, 2015.

[31] H. W. Engl, M. Hanke, and A. Neubauer. *Regularization of inverse problems*. Kluwer Academic Publishers, 1996.

[32] H. Garde. Reconstruction of piecewise constant layered conductivities in electrical impedance tomography. *Communications in Partial Differential Equations*, 45(9):1118–1133, 2020.

[33] H. Garde and S. Staboulis. Convergence and regularization for monotonicity-based shape reconstruction in electrical impedance tomography. *Numerische Mathematik*, 135(4):1221–1251, 2017.

[34] H. Garde and S. Staboulis. The regularized monotonicity method: Detecting irregular indefinite inclusions. *Inverse Problems & Imaging*, 13(1):93–116, 2019.

[35] B. Gebauer. The factorization method for real elliptic problems. *Zeitschrift für Analysis und ihre Anwendungen*, 25(1):81–102, 2006.

[36] B. Gebauer. Localized potentials in electrical impedance tomography. *Inverse Problems & Imaging*, 2(2):251–269, 2008.

[37] B. Gebauer and N. Hyvönen. Factorization method and irregular inclusions in electrical impedance tomography. *Inverse Problems*, 23(5):2159, 2007.

[38] D. Gilbarg and N. S. Trudinger. *Elliptic partial differential equations of second order*. Springer, 2015.

[39] B. Haberman and D. Tataru. Uniqueness in Calderón's problem with Lipschitz conductivities. *Duke Mathematical Journal*, 162(3):497–516, 2013.

[40] J. Hadamard. Lectures on the Cauchy Problem in Linear Partial Differential Equations. *Differential Equations*, 1923.

[41] S. J. Hamilton, A. Hänninen, A. Hauptmann, and V. Kolehmainen. Beltrami-net: domain-independent deep D-bar learning for absolute imaging with electrical impedance tomography (a-EIT). *Physiological Measurement*, 40(7):074002, 2019.

[42] S. J. Hamilton and A. Hauptmann. Deep D-bar: Real-time electrical impedance tomography imaging with deep neural networks. *IEEE Transactions on Medical Imaging*, 37(10):2367–2377, 2018.

[43] L. Harhanen, N. Hyvönen, H. Majander, and S. Staboulis. Edge-enhancing reconstruction algorithm for three-dimensional electrical impedance tomography. *SIAM Journal on Scientific Computing*, 37(1):B60–B78, 2015.

[44] B. Harrach. Recent progress on the factorization method for electrical impedance tomography. *Computational and Mathematical Methods in Medicine*, 2013, 2013.

[45] B. Harrach. Uniqueness and Lipschitz stability in electrical impedance tomography with finitely many electrodes. *Inverse Problems*, 35(2):024005, 2019.

[46] B. Harrach and M. Ullrich. Monotonicity-based shape reconstruction in electrical impedance tomography. *SIAM Journal on Mathematical Analysis*, 45(6):3382–3403, 2013.

[47] B. Harrach and M. Ullrich. Resolution guarantees in electrical impedance tomography. *IEEE Transactions on Medical Imaging*, 34(7):1513–1521, 2015.

[48] X. He, K. Zhao, and X. Chu. AutoML: A Survey of the State-of-the-Art. *Knowledge-Based Systems*, 212:106622, 2021.

[49] R. P. Henderson and J. G. Webster. An impedance camera for spatially specific measurements of the thorax. *IEEE Transactions on Biomedical Engineering*, BME-25(3):250–254, 1978.

[50] M. Hintermüller and T. Wu. Nonconvex TV^q-models in image restoration: Analysis and a trust-region regularization–based superlinearly convergent solver. *SIAM Journal on Imaging Sciences*, 6(3):1385–1415, 2013.

[51] D. S. Holder. Feasibility of developing a method of imaging neuronal activity in the human brain: a theoretical review. *Medical and Biological Engineering and Computing*, 25(1):2–11, 1987.

[52] N. Hyvönen. Complete electrode model of electrical impedance tomography: Approximation properties and characterization of inclusions. *SIAM Journal on Applied Mathematics*, 64(3):902–931, 2004.

[53] N. Hyvönen, V. Kaarnioja, L. Mustonen, and S. Staboulis. Polynomial collocation for handling an inaccurately known measurement configuration in electrical impedance tomography. *SIAM Journal on Applied Mathematics*, 77(1):202–223, 2017.

[54] N. Hyvönen and L. Mustonen. Smoothened complete electrode model. *SIAM Journal on Applied Mathematics.*, 77(6):2250–2271, 2017.

[55] N. Hyvönen and L. Mustonen. Generalized linearization techniques in electrical impedance tomography. *Numerische Mathematik*, 140(1):95–120, 2018.

[56] M. Ikehata. How to draw a picture of an unknown inclusion from boundary measurements. Two mathematical inversion algorithms. *Journal of Inverse and Ill-Posed Problems*, 7:255–272, 1999.

[57] M. Ikehata. Reconstruction of the support function for inclusion from boundary measurements. *Journal of Inverse and Ill-Posed Problems*, 8(4):367–378, 2000.

[58] O. Imanuvilov, G. Uhlmann, and M. Yamamoto. The Calderón problem with partial data in two dimensions. *Journal of the American Mathematical Society*, 23(3):655–691, 2010.

[59] M. Jehl, J. Avery, E. Malone, D. S. Holder, and T. Betcke. Correcting electrode modelling errors in EIT on realistic 3D head models. *Physiological Measurement*, 36(12):2423, 2015.

[60] J. P. Kaipio and E. Somersalo. *Statistical and Computational Inverse Problems*. Springer, 2005.

[61] N. Kanwar, A. K. Goswami, and S. P. Mishra. Design Issues in Artificial Neural Network (ANN). In *2019 4th International Conference on Internet of Things: Smart Innovation and Usages (IoT-SIU)*, pages 1–4, 2019.

[62] C. Kenig, J. Sjöstrand, and G. Uhlmann. The Calderón problem with partial data. *Annals of Mathematics*, pages 567–591, 2007.

[63] A. Kirsch. Characterization of the shape of a scattering obstacle using the spectral data of the far field operator. *Inverse Problems*, 14(6):1489, 1998.

[64] A. Kirsch and N. Grinberg. *The factorization method for inverse problems*. Oxford University Press, 2008.

[65] R. Kohn and M. Vogelius. Determining conductivity by boundary measurements. *Communications on Pure and Applied Mathematics*, 37(3):289–298, 1984.

[66] V. Kolehmainen, M. Lassas, and P. Ola. The inverse conductivity problem with an imperfectly known boundary. *SIAM Journal on Applied Mathematics*, 66(2):365–383, 2005.

[67] V. Kolehmainen, M. Lassas, and P. Ola. The inverse conductivity problem with an imperfectly known boundary in three dimensions. *SIAM Journal on Applied Mathematics*, 67(5):1440–1452, 2007.

[68] A. Lechleiter and A. Rieder. Newton regularizations for impedance tomography: a numerical study. *Inverse Problems*, 22(6):1967, 2006.

[69] A. Lechleiter and A. Rieder. Newton regularizations for impedance tomography: convergence by local injectivity. *Inverse Problems*, 24(6):065009, 2008.

[70] Y. LeCun, Y. Bengio, and G. Hinton. Deep learning. *Nature*, 521(7553):436–444, 2015.

[71] E. G. Lee, W. Duffy, R. L. Hadimani, M. Waris, W. Siddiqui, F. Islam, M. Rajamani, R. Nathan, and D. C. Jiles. Investigational effect of brain-scalp distance on the efficacy of transcranial magnetic stimulation treatment in depression. *IEEE Transactions on Magnetics*, 52(7):1–4, 2016.

[72] X. Li, Y. Zhou, J. Wang, Q. Wang, Y. Lu, X. Duan, Y. Sun, J. Zhang, and Z. Liu. A novel deep neural network method for electrical impedance tomography. *Transactions of the Institute of Measurement and Control*, 41(14):4035–4049, 2019.

[73] A. Lucas, M. Iliadis, R. Molina, and A. K. Katsaggelos. Using deep neural networks for inverse problems in imaging: beyond analytical methods. *IEEE Signal Processing Magazine*, 35(1):20–36, 2018.

[74] M. T. McCann, K. H. Jin, and M. Unser. Convolutional neural networks for inverse problems in imaging: A review. *IEEE Signal Processing Magazine*, 34(6):85–95, 2017.

[75] A. Nachman. Global uniqueness for a two-dimensional inverse boundary value problem. *Annals of Mathematics*, pages 71–96, 1996.

[76] A. Nachman, I. Regev, and D. Tataru. A nonlinear Plancherel theorem with applications to global well-posedness for the defocusing Davey–Stewartson equation and to the inverse boundary value problem of Calderón. *Inventiones Mathematicae*, 220(2):395–451, 2020.

[77] A. Nissinen, L. M. Heikkinen, V. Kolehmainen, and J. P. Kaipio. Compensation of errors due to discretization, domain truncation and unknown contact impedances in electrical impedance tomography. *Measurement Science and Technology*, 20(10):105504, 2009.

[78] A. Nissinen, V. Kolehmainen, and J. P. Kaipio. Reconstruction of domain boundary and conductivity in electrical impedance tomography using the approximation error approach. *International Journal for Uncertainty Quantification*, 1(3), 2011.

[79] L. Päivärinta, A. Panchenko, and G. Uhlmann. Complex geometrical optics solutions for Lipschitz conductivities. *Revista Matematica Iberoamericana*, 19(1):57–72, 2003.

[80] P. Perona and J. Malik. Scale-space and edge detection using anisotropic diffusion. *IEEE Transactions on Pattern Analysis and Machine Intelligence*, 12(7):629–639, 1990.

[81] M. K. Pidcock, M. Kuzuoglu, and K. Leblebicioglu. Analytic and semi-analytic solutions in electrical impedance tomography: I. Two-dimensional problems. *Physiological Measurement*, 16(2):77–90, 1995.

[82] M. K. Pidcock, M. Kuzuoglu, and K. Leblebicioglu. Analytic and semi-analytic solutions in electrical impedance tomography: II. Three-dimensional problems. *Physiological Measurement*, 16(2):91, 1995.

[83] J. L. Saver. Time is brain quantified. *Stroke*, 37(1):263–266, 2006.

[84] J. Schmidhuber. Deep learning in neural networks: An overview. *Neural Networks*, 61:85–117, 2015.

[85] J. K. Seo, K. C. Kim, A. Jargal, K. Lee, and B. Harrach. A learning-based method for solving ill-posed nonlinear inverse problems: a simulation study of lung EIT. *SIAM Journal on Imaging Sciences*, 12(3):1275–1295, 2019.

[86] J. R. Shewchuk. Triangle: Engineering a 2D quality mesh generator and Delaunay triangulator. In *Applied Computational Geometry Towards Geometric Engineering*, pages 203–222. Springer, 1996.

[87] H. Si. TetGen, a Delaunay-based quality tetrahedral mesh generator. *ACM Transactions on Mathematical Software (TOMS)*, 41(2):1–36, 2015.

[88] S. Siltanen, J. Mueller, and D. Isaacson. An implementation of the reconstruction algorithm of A. Nachman for the 2D inverse conductivity problem. *Inverse Problems*, 16(3):681, 2000.

[89] E. Somersalo, M. Cheney, and D. Isaacson. Existence and uniqueness for electrode models for electric current computed tomography. *SIAM Journal on Applied Mathematics*, 52(4):1023–1040, 1992.

[90] G. Strang and G. J. Fix. *An analysis of the finite element method*. Prentice-hall, 1973.

[91] A. M. Stuart. Inverse problems: a Bayesian perspective. *Acta Numerica*, 19:451–559, 2010.

[92] J. Sylvester. An anisotropic inverse boundary value problem. *Communications on Pure and Applied Mathematics*, 43(2):201–232, 1990.

[93] J. Sylvester and G. Uhlmann. A global uniqueness theorem for an inverse boundary value problem. *Annals of Mathematics*, pages 153–169, 1987.

[94] A. Tamburrino and G. Rubinacci. A new non-iterative inversion method for electrical resistance tomography. *Inverse Problems*, 18(6):1809, 2002.

[95] G. Uhlmann. Electrical impedance tomography and Calderón's problem. *Inverse Problems*, 25(12):123011, 2009.

[96] M. Vauhkonen. *Electrical impedance tomography with prior information*, volume 62. Kuopio University Publications C (Dissertation), 1997.

[97] M. Vauhkonen, D. Vadasz, P. A. Karjalainen, E. Somersalo, and J. P. Kaipio. Tikhonov regularization and prior information in electrical impedance tomography. *IEEE Transactions on Medical Imaging*, 17(2):285–293, 1998.

[98] T. Vilhunen, J. P. Kaipio, P. J. Vauhkonen, T. Savolainen, and M. Vauhkonen. Simultaneous reconstruction of electrode contact impedances and internal electrical properties: I. theory. *Measurement Science and Technology*, 13(12):1848, 2002.

[99] C. R. Vogel and M. E. Oman. Iterative methods for total variation denoising. *SIAM Journal on Scientific Computing*, 17(1):227–238, 1996.

[100] L. Yang, W. Liu, R. Chen, G. Zhang, W. Li, F. Fu, and X. Dong. In Vivo Bioimpedance spectroscopy characterization of healthy, hemorrhagic and ischemic rabbit brain within 10 Hz–1 MHz. *Sensors*, 17(4):791, 2017.

Aalto-DD 139/2021

ISBN 978-952-64-0544-5 (printed)
ISBN 978-952-64-0545-2 (pdf)
ISSN 1799-4934 (printed)
ISSN 1799-4942 (pdf)

Aalto University
School of Science
Department of Mathematics and Systems Analysis
www.aalto.fi

BUSINESS +
ECONOMY

ART +
DESIGN +
ARCHITECTURE

SCIENCE +
TECHNOLOGY

CROSSOVER

**DOCTORAL
DISSERTATIONS**